



Iron–cobalt mixed oxide nanocatalysts: Heterogeneous peroxyomonosulfate activation, cobalt leaching, and ferromagnetic properties for environmental applications

Qijing Yang ^a, Hyeok Choi ^b, Souhail R. Al-Abed ^{b,*}, Dionysios D. Dionysiou ^{a,**}

^a Department of Civil and Environmental Engineering, University of Cincinnati, Cincinnati, OH 45221-0071, United States

^b National Risk Management Research Laboratory, U.S. Environmental Protection Agency, 26W. Martin Luther King Dr., Cincinnati, OH 45268, United States

ARTICLE INFO

Article history:

Received 25 June 2008

Received in revised form 17 October 2008

Accepted 21 October 2008

Available online 31 October 2008

Keywords:

2,4-Dichlorophenol

Advanced oxidation processes (AOPs)

Advanced oxidation technologies (AOTs)

Cobalt

Fe–Co

Ferromagnetic properties

Heterogeneous reaction

Iron

Iron–cobalt

Leaching

Mixed oxide

Nanoparticles

Oxone

Peroxyomonosulfate

Support materials

Sulfate radicals

Titanium dioxide

Titania

TiO₂

Water treatment

Water purification

ABSTRACT

Sulfate radical-based advanced oxidation technologies (SR-AOTs) are attracting considerable attention due to the high oxidizing ability of SRs to degrade organic pollutants in aqueous environments. This study was carried out to respond to current concerns and challenges in SR-AOTs, including (i) need of heterogeneous activation of sulfate salts using transition metal oxides, (ii) nanoscaling of the metal oxide catalysts for high catalytic activity and promising properties with respect to leaching, and (iii) easy removal and recovery of the catalytic materials after their applications for water and wastewater treatments. In this study, we report a novel approach of using Fe–Co mixed oxide nanocatalysts for the heterogeneous activation of peroxyomonosulfate (PMS) to generate SRs targeting the decomposition of 2,4-dichlorophenol, and especially focus on some synthesis parameters such as calcination temperature, Fe/Co contents, and TiO₂ support. The physicochemical properties of the catalysts were investigated using porosimetry, XRD, HR-TEM, H₂-TPR, and XPS. Ferromagnetic CoFe₂O₄ composites formed by thermal oxidation of a mixed phase of Fe and Co exhibited significant implications for the efficient and environmentally friendly activation of PMS, including (i) the cobalt species in CoFe₂O₄ are of Co(II), unlike Co₃O₄ showing some detrimental effects of Co(III) on the PMS activation, (ii) CoFe₂O₄ possesses suppressed Co leaching properties due to strong Fe–Co interactions (i.e. Fe–Co linkages), and (iii) Fe–Co catalysts in form of CoFe₂O₄ are easier to recover due to the unique ferromagnetic nature of CoFe₂O₄. In addition, the presence of Fe was found to be beneficial for enriching hydroxyl group content on the Fe–Co catalyst surface, which is believed to facilitate the formation of Co(II)–OH complexes that are vital for heterogeneous PMS activation.

© 2008 Elsevier B.V. All rights reserved.

1. Introduction

In general, advanced oxidation technologies (AOTs) are based on the activation of oxidants such as hydrogen peroxide and ozone to generate highly oxidizing transient species such as hydroxyl radicals (HRs, •OH) [1]. Semiconductor materials such as TiO₂ are

also able to generate HRs when irradiated with high photon energy above their band gap, typically by ultraviolet (UV). Among various AOTs, Fenton reagent (e.g. Fe²⁺ + H₂O₂) and photocatalysis (e.g. TiO₂ + UV) have been intensively investigated for environmental applications during the last decades because of their promising performances in the degradation of many pollutants in water and wastewater [2–5]. However, the Fenton reagent requires an acidic pH condition close to 3 while TiO₂ photocatalysis needs UV irradiation in most cases [2,3]. These requirements and some other issues remarkably limit their practical applications [6]. Compared to HRs with standard reduction potential of 1.8–2.7 V, sulfate radicals (SRs, SO₄²⁻) also demonstrate high reduction potential of

* Corresponding author. Tel.: +1 513 569 7849; fax: +1 513 569 7879.

** Corresponding author. Tel.: +1 513 556 0724; fax: +1 513 556 2599.

E-mail addresses: al-abed.souhail@epa.gov (S.R. Al-Abed),

dionysios.d.dionysiou@uc.edu (D.D. Dionysiou).

2.5–3.1 V at neutral pH and are more selective for oxidation [7]. Recently, many research studies have been conducted to find an alternative and practical approach employing SR-based technologies to the traditional AOTs [8–15].

In general, SRs are generated via homogeneous activation of peroxyomonosulfate (PMS) with transition metal ions, among which cobalt is the best activator [14]. As expected, this homogeneous approach is highly efficient to degrade water pollutants. However, aesthetic aspects and health concerns associated with the adverse effect of dissolved cobalt species in water still need to be addressed. Anipsitakis et al. first demonstrated the heterogeneous PMS activation using commercially available Co_3O_4 particles [12]. More recently, in order to increase the reactivity of the catalyst, we immobilized and distributed nanosized Co_3O_4 particles onto various support materials, among which TiO_2 was proven the most efficient for limiting the cobalt leaching due to strong metal-support (Co-Ti) interactions [8,9]. Moreover, in comparison with the commercially available bulk Co_3O_4 , the $\text{Co}_3\text{O}_4/\text{TiO}_2$ system exhibited a much higher efficiency for the PMS activation due to its engineered properties at nanoscale [8]. However, the absence of practical and efficient approaches to recover the nanosized $\text{Co}_3\text{O}_4/\text{TiO}_2$ catalyst is a bottleneck for its environmental applications since nanosized materials, when discharged, might cause secondary environmental problems [16–18].

Consequently, it is critical to develop a highly efficient nanoscale metal catalyst for the heterogeneous PMS activation, where the adverse impact of metal leaching on aqueous environments is notably minimized and the catalyst is readily recovered after its application. Considering the environmental and practical aspects, Fe as a candidate for the catalyst might be more relevant than Co. However, the efficiency of $\text{Fe}(\text{II})$ ions, as well as Fe_2O_3 , which can be typically formed during heat treatment of Fe salts, were found to be inferior for the activation of PMS to degrade 2,4-dichlorophenol (2,4-DCP) [14]. Coupling of Fe with a suitable amount of Co (i.e. Fe-Co mixed oxide catalysts) might be an effective way to attain efficient catalysts for PMS activation. In addition, the cobalt leaching from the Fe-Co catalysts can be controlled since strong metal–metal interactions are typically observed during their heat treatment. Moreover, under appropriate conditions, the nanocomposite catalysts can be transformed to CoFe_2O_4 which can be easily recovered using magnetic-based separation due to its ferromagnetic properties [19].

In this study, we report the development of a novel approach of using Fe-Co mixed oxide nanocatalysts as a mediator for the heterogeneous PMS activation. We focus on the effect of several factors such as cobalt content, calcination temperature, and TiO_2 support for the Fe-Co catalysts on cobalt leaching, Fe-Co interaction, and heterogeneous activation of PMS. The catalyst performance was evaluated in terms of the degradation of highly toxic and poorly biodegradable 2,4-DCP, which mainly originates from the environmental transformation of herbicides such as 2,4-dichlorophenoxyacetic acid [13]. Moreover, we discuss the environmentally friendly aspects of the Fe-Co nanocatalysts, including reduced cobalt leaching and ferromagnetic-based separation properties.

2. Experimental

2.1. Catalyst preparation

Fe-Co mixed oxide nanocatalysts were synthesized via thermal oxidation of Fe and Co salts. Desired amounts of $\text{Fe}(\text{NO}_3)_3 \cdot 9\text{H}_2\text{O}$ (98+, Sigma) and $\text{Co}(\text{NO}_3)_2 \cdot 6\text{H}_2\text{O}$ (99.3%, Sigma) were mixed in super quality water ($18\text{ M}\Omega$) under vigorous stirring. This suspension was stirred for 24 h, and then dried under an infrared lamp at around 50 °C. The as-prepared catalysts were calcined in a

furnace (Paragon model HT-22D, Thermcraft) at 300–700 °C in air for 4 h with a ramp rate of 10 °C/min. Bulk Co_3O_4 and Fe_2O_3 were also synthesized independently, and then calcined at 500 °C for 4 h. In addition, immobilized Fe–Co catalysts on TiO_2 support were synthesized by wet impregnation employing the iron and cobalt nitrate precursors mixed with 30 nm TiO_2 nanoparticles (Degussa P-25, anatase/rutile mixture) at the molar ratio of $\text{Fe}:\text{Co}:\text{TiO}_2$ of 1:1:20 [9]. The resulting Fe–Co catalysts were ground thoroughly and labeled as $X\text{Fe}Y\text{Co}Z$, where X/Y stands for the molar ratio of Fe/Co and Z denotes the calcination temperature. Similarly, the supported Fe–Co catalysts on TiO_2 were referred to as $\text{FeCo}/\text{TiO}_2Z$. As a comparison, an immobilized Co catalyst on TiO_2 at a Co/Ti molar ratio of 0.1 (0.1Co/ TiO_2) was fabricated following the procedure described elsewhere [8].

2.2. Catalyst characterization

The crystallographic structure of the catalysts was investigated with X-ray diffraction (XRD) analysis using a Kristalloflex D500 diffractometer (Siemens) with $\text{Cu K}\alpha$ ($\lambda = 1.5406\text{ \AA}$) radiation. The crystalline size B was estimated from the width of lines in the X-ray pattern with the aid of the Scherrer formula: $B = 0.9\lambda/(\beta \times \cos \theta)$, where λ is the wavelength of the X-ray used, β is the width of the line at the half-maximum intensity, and θ is the diffraction peak angle. The elemental composition and electronic structure of Co–Fe catalysts were investigated by X-ray photoelectron spectroscopy (XPS, PerkinElmer Model 5300) using $\text{Mg K}\alpha$ X-rays. During analysis, the pressure was kept between 10^{-8} and 10^{-9} Torr. Charge correction was performed by referencing the C 1s peak for hydrocarbons to a binding energy of 284.6 eV. Curve fitting of the XPS spectra was accomplished using a combination of 90% Gaussian and 10% Lorentzian peak shape. Atomic concentrations were obtained from the XPS spectra based on peak areas and sensitivity factors provided by the software (RBD Enterprises, Bend, OR, USA). The morphology of the catalysts was characterized by a JEM-2010F (JEOL) high resolution-transmission electron microscope (HR-TEM) with field emission gun at 200 kV. The samples were dispersed in methanol using an ultrasonicator for 5 min and fixed on a carbon-coated copper grid (LC200-Cu, EMS). H_2 -temperature programmed reduction (H_2 -TPR) was conducted on a Micromeritics AutoChem 2910 TPD/TPR instrument. About 0.3 g of sample was loaded into a quartz reactor and heated at a heating rate of 10 °C/min in a stream of 5% H_2 in Ar with a flow rate of 20 mL/min up to 800 °C. H_2 consumption upon iron and/or cobalt reduction was monitored by a thermal conductivity detector. A Tristar 3000 (Micromeritics) surface area and porosimetry analyzer was used to determine the Brunauer–Emmett–Teller (BET) surface area (S_{BET}) of the catalysts. The samples were purged with nitrogen gas for 2 h at 150 °C using SmartPrep programmable degas system (Micromeritics).

2.3. Evaluation of catalytic activity

A quartz reactor (base: 10 cm × 10 cm; height: 25 cm) containing 1 L of 50 mg/L (0.307 mM) 2,4-DCP solution with adjusted pH of 7.0 using K_2HPO_4 and KHSO_4 was stirred vigorously on a magnetic plate. No obvious 2,4-DCP volatilization was observed in a control experiment. After the addition of 0.1 g Fe–Co catalyst into the 2,4-DCP solution, the suspension was allowed to reach adsorption equilibrium between the catalyst and aqueous phases (there was negligible 2,4-DCP adsorption on the catalyst surface). Then, Oxone (KHSO_5 as active component, Aldrich, manufactured by DuPont) was added into the solution at a $\text{KHSO}_5/2,4\text{-DCP}$ molar ratio of 3:1. For the measurement of 2,4-DCP concentrations during 2 h of reaction, 10 mL sample was taken at specific time intervals

and quenched with 5 mL of 2.47 M methanol (Aldrich) to prevent further reaction. The sample was filtered with 0.1 μm filter (Magna Nylon, Fischer) and analyzed using a high performance liquid chromatograph (HPLC, Agilent 1100 Series) with a photo-diode-array detector. The column was an Eclipse XDBC8 column (Agilent) and mobile phase was 70:30% (v/v) of 0.01 N H_2SO_4 :acetonitrile. An atomic absorption spectrometer (PerkinElmer AA-300) was used to study Co leaching to the solution.

3. Results and discussion

3.1. Textural property and crystal phase

Table 1 summarizes the S_{BET} and crystallographic properties of Fe-Co catalysts. The S_{BET} of Fe-Co catalysts decreased with increasing calcination temperature because of the crystalline growth of Co_3O_4 and Fe_2O_3 so that all the Fe-Co catalysts calcined at 700 °C showed very similar S_{BET} values between 3 and 4 m^2/g . **Fig. 1** presents the XRD patterns of 1Fe1Co catalysts calcined at different temperatures. Only Fe_2O_3 (JCPDS 33-0664) and Co_3O_4 (JCPDS 42-1467) phases were clearly observed in the Fe-Co catalysts prepared at 300 and 500 °C. The weak XRD peaks of 1Fe1Co300 indicate small crystallite sizes of Co_3O_4 and Fe_2O_3 . Since it was reported in a previous study that calcination above 450 °C is required to fully convert metal nitrates to the corresponding metal oxides [20], the catalyst prepared at 300 °C might have unconverted iron and cobalt nitrate precursors. However, their quantity in 1Fe1Co300 was too low to be identified through XRD peak analysis. As shown in **Fig. 2**, FeCo700 catalysts with different Fe/Co molar ratios showed some intensive peaks attributed to CoFe_2O_4 (JCPDS 22-1086) in addition to Fe_2O_3 and Co_3O_4 . CoFe_2O_4 is a mixed metal oxide spinel (general formulation: AB_2O_4) with Co^{2+} in the tetrahedral "A" sites and Fe^{3+} in the octahedral "B" sites in a face-centered cubic crystalline structure [19]. Heat treatment of the Fe-Co catalysts can result in the intimate solid–solid interaction between the Co–Fe interface and then diffusion with each other to generate CoFe_2O_4 spinel structure [19]. Recently, Kim et al. studied the various linkages (i.e. Co–Co, Fe–Fe, and Co–Fe) in CoFe_2O_4 , and reported that among them the Co–Fe interaction is the strongest [21]. Hence, the formation of abundant CoFe_2O_4 spinel structure in the FeCo700 catalysts is inferred to result from strong interaction between Fe(III) and Co(II) at the molecular level (i.e. Fe–Co linkages). On the other hand, two separated phases (i.e. Fe_2O_3 and Co_3O_4) exist in 1Fe1Co300 and 1Fe1Co500, where only small amount of Fe–Co linkages might be formed at the interface of the two phases, making their Fe–Co interactions much weaker than those in FeCo700. 1Fe1Co700 and 3Fe7Co700 had cobalt in forms of Co_3O_4 and CoFe_2O_4 while 7Fe3Co700 showed the strongest CoFe_2O_4 peaks and no Co_3O_4 peaks, indicating that all the cobalt species were converted to CoFe_2O_4 . The formation of different cobalt compounds (i.e. Co_3O_4 and CoFe_2O_4) in the Fe–Co catalysts can substantially affect their catalytic performance, cobalt leaching, and recovery behavior

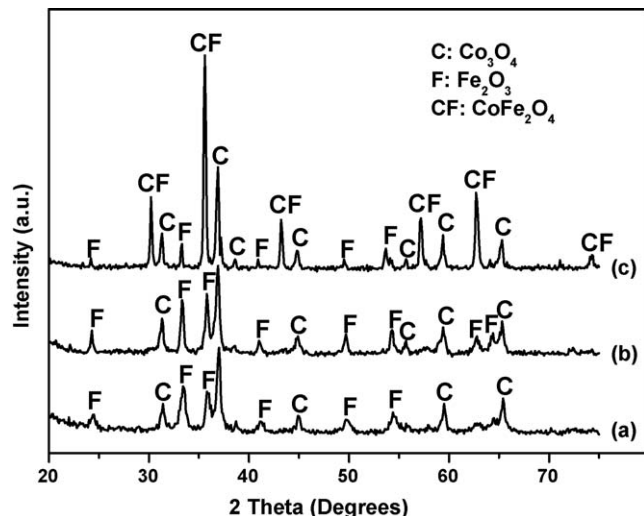


Fig. 1. XRD patterns of (a) 1Fe1Co300, (b) 1Fe1Co500, and (c) 1Fe1Co700.

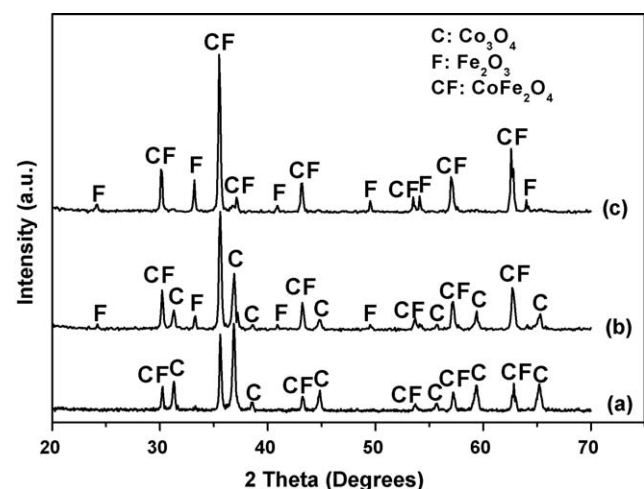


Fig. 2. XRD patterns of (a) 3Fe7Co700, (b) 1Fe1Co700, and (c) 7Fe3Co700.

because: (i) Co species in CoFe_2O_4 is of Co(II) while that in Co_3O_4 is a mixture of Co(II) and Co(III) with Co(III) being predominant (the molar ratio of Co(III)/Co(II) is 2), (ii) CoFe_2O_4 is expected to possess more intimate Fe–Co interactions than just the mixture of Co_3O_4 and Fe_2O_3 , and (iii) interestingly CoFe_2O_4 has exceptional ferromagnetic properties.

The crystalline sizes of Co_3O_4 , Fe_2O_3 , and CoFe_2O_4 in the Fe–Co catalysts are listed in **Table 1**. For 1Fe1Co, slight crystal growth of Co_3O_4 from 28.7 to 32.4 nm was observed with increasing calcination temperature from 500 to 700 °C. The result is some-

Table 1
Surface area, crystallographic properties, and XPS analysis results of Fe–Co catalysts.

Catalysts	S_{BET} (m^2/g)	Crystalline size (nm) ^a			Elemental composition (atomic %)			$\text{O}_\text{H}/(\text{O}_\text{H} + \text{O}_\text{L})^\text{b}$ (%)
		Co_3O_4	Fe_2O_3	CoFe_2O_4	Fe	Co	O	
1Fe1Co300	42.2	25.6	16.2	–	–	–	–	–
1Fe1Co500	10.1	28.7	28.0	–	12.7	23.4	63.9	18.2
1Fe1Co700	3.7	32.4	42.7	36.7	16.8	18.8	64.3	11.0
3Fe7Co700	3.4	37.5	–	38.8	12.0	24.1	63.9	8.6
7Fe3Co700	3.4	–	51.2	39.4	24.6	11.2	64.2	16.1

^a (1 0 1) for anatase TiO_2 , (1 1 0) for rutile TiO_2 , (2 2 0) for Co_3O_4 , and (1 0 4) for CoTiO_3 .

^b O_H and O_L stand for surface hydroxyl oxygen and lattice oxygen, respectively.

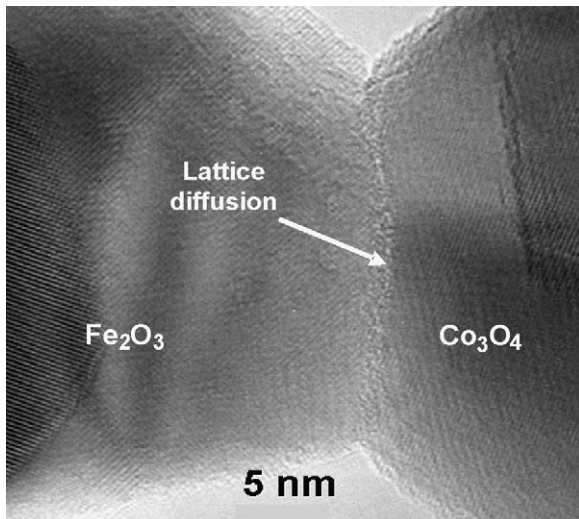


Fig. 3. HR-TEM images of 1Fe1Co500.

what different from our previous finding showing that the crystalline size of cobalt species immobilized onto TiO_2 was significantly increased from 30 to 40 nm at 500 °C to ~70 nm at 700 °C [9]. This discrepancy implies that the intimate Fe–Co interactions resulting from the formation of CoFe_2O_4 were more efficient for suppressing the growth of crystalline cobalt. Fig. 3 presents the HR-TEM image of 1Fe1Co500. Clear lattice fringes revealed the crystal characteristics of 1Fe1Co500 comprised of Co_3O_4 and Fe_2O_3 particles. The value of d_{space} at 0.46 nm corresponds to the (1 1 1) plane of Co_3O_4 while that at 0.37 nm corresponds to the (0 1 2) plane of Fe_2O_3 [22]. Moreover, we can clearly see fusion of the Fe_2O_3 to Co_3O_4 lattices at their grain boundaries, suggesting the existence of intimate Fe–Co interactions (Fe–Co linkages) in 1Fe1Co500.

3.2. H_2 -TPR and Fe–Co interaction

In order to investigate the metal–metal interactions in Fe–Co catalysts, which are likely to have profound impacts on their catalytic performances and leaching behavior, H_2 -TPR analysis was applied to 1Fe1Co catalysts as well as the bulk Fe_2O_3 and Co_3O_4 , as shown in Fig. 4. The bulk Fe_2O_3 showed a sharp peak at 360 °C

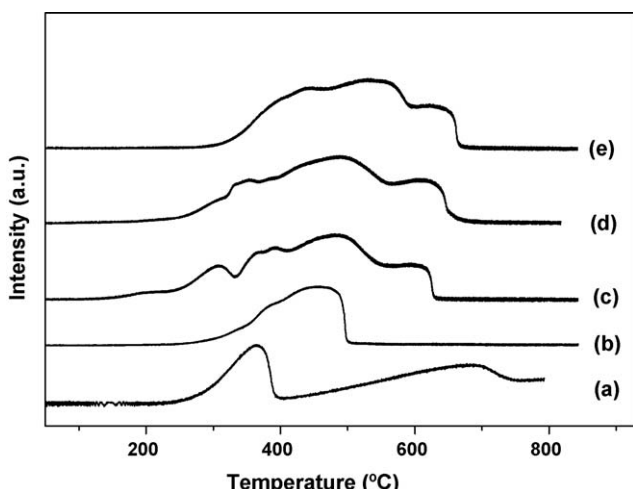


Fig. 4. TPR profiles of (a) Fe_2O_3 , (b) Co_3O_4 , (c) 1Fe1Co300, (d) 1Fe1Co500, and (e) 1Fe1Co700.

assigned to the reduction of Fe_2O_3 to Fe_3O_4 and a broad signal at 680 °C corresponding to subsequent reduction of Fe_3O_4 to Fe^0 [23]. In the case of Co_3O_4 , the intensive peak between 300 and 500 °C is explained by the overlapping of two reduction steps: $\text{Co}_3\text{O}_4 \rightarrow \text{CoO} \rightarrow \text{Co}^0$ [24]. TPR profiles of the Fe–Co systems are relatively complex. 1Fe1Co300 has four obvious reduction peaks at ~300, 390, 475, and 600 °C. Based on the XRD results suggesting the presence of unconverted metal nitrate precursors in this catalyst, the peak at 300 °C might have been derived from the reduction of the residual nitrate precursors [25]. The reduction peaks at 390 and 600 °C result from the sequential reduction of Fe_2O_3 to Fe_3O_4 followed by Fe^0 , while the peak at 475 °C is assigned to the reduction of Co_3O_4 to Co^0 . TPR of 1Fe1Co500 exhibited quite similar behavior to that of 1Fe1Co300 except the disappearance of the peak at ~300 °C due to the complete conversion of the metal nitrate precursors to the corresponding metal oxides upon calcination at 500 °C. The reduction peaks of 1Fe1Co700 notably shifted to high temperatures, indicating that calcination at 700 °C can give rise to significant changes of catalyst structure and thereby make it more difficult to be reduced. This is due to the generation of more intimate Fe–Co interactions in 1Fe1Co700 as a result of the formation of CoFe_2O_4 .

3.3. Elemental composition and electronic structure

XPS analysis results on the elemental composition of the Fe–Co catalyst surface and contents of surface hydroxyl groups are summarized in Table 1. Fe and Co contents on the catalyst surfaces notably varied whereas the oxygen content was stable at around 64%. Interestingly, Co content on the surface of 1Fe1Co500 is 23.4%, which is about two times higher than Fe content although their stoichiometric ratio should be one. Due to the analysis depth of XPS (≤ 10 nm), the high ratio of Co to Fe demonstrates that the surface of 1Fe1Co500 was Co_3O_4 -rich phase. This phenomenon might be attributed to the fact that in the case of 1Fe1Co300, the crystalline growth of Co_3O_4 was faster than that of Fe_2O_3 , justified by the larger crystalline size of Co_3O_4 (25.6 nm) as compared with that of Fe_2O_3 (16.2 nm). Thus, Co_3O_4 particles could probably cover more catalyst surface than Fe_2O_3 particles. Meanwhile, it should be noted that 1Fe1Co700 exhibited a Fe/Co ratio very close to 1 with the remarkable growth of Fe_2O_3 crystallites to 42.7 nm. By contrast, the size of Co_3O_4 crystallites was slightly increased to 32.4 nm. This implies that calcination at 700 °C promoted the growth of Fe_2O_3 crystallites, which led to structure rearrangement of Fe–Co catalyst to achieve more uniform distribution of Co and Fe on the surface of the 1Fe1Co700 catalyst. It has been reported that the calcination process could result in particle adhesion (grain growth), diffusion of ions of the solid along the outermost surface layer of the lattice, thereby filling cracks and surface irregularities [26]. We strongly believe that in this study the calcination process would facilitate the formation of more intimate Fe–Co interactions as demonstrated in H_2 -TPR analysis.

Fig. 5(a) shows XPS result of $\text{Co } 2p_{3/2}$ core level for the 7Fe3Co700 catalyst. The spectrum was well fitted with three peaks. The peak at 782.1 eV resulted from a chemical shift of the main spin orbit components because the Co cations on the nanocrystal surface are chemically interacted with surface hydroxyls which correspond to the shake-up satellite observed at 786.1 eV [27]. Interestingly, 7Fe3Co700 did not show a shake-up satellite of $\text{Co } 2p_{3/2}$ at 789.0 eV that is characteristic of Co(III) [27] while this peak could be clearly identified in 1Fe1Co500, 1Fe1Co700, and 3Fe7Co700 catalysts as shown in Fig. 5(b)–(d). This confirms that all cobalt species in 7Fe3Co700 existed as Co(II). Clearly, the XRD, H_2 -TPR, and XPS results strongly support that the cobalt species in

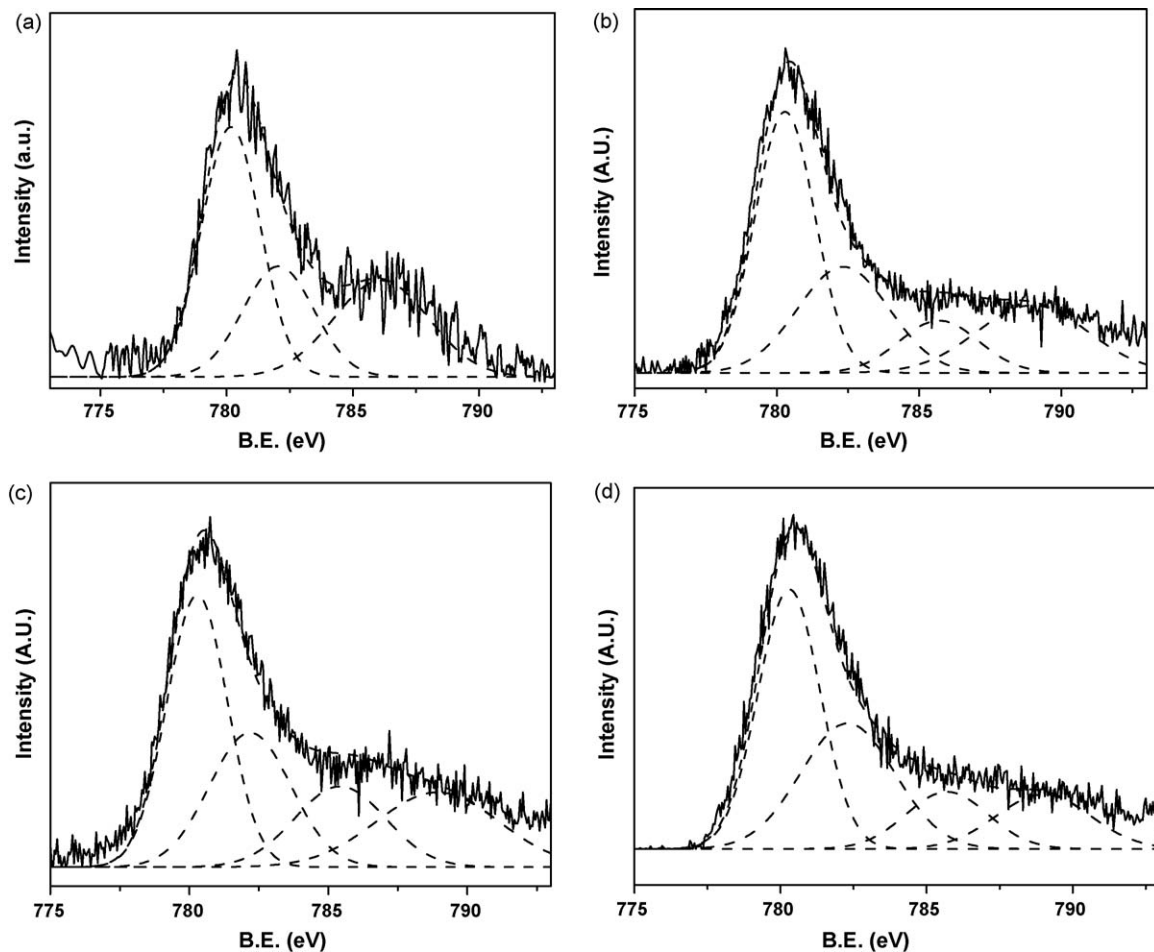


Fig. 5. XPS spectra of Co 2p_{3/2} for (a) 7Fe3Co700, (b) 1Fe1Co500, (c) 1Fe1Co700, and (d) 3Fe7Co700.

7Fe3Co700 were effectively coupled with the iron to form CoFe₂O₄ with intimate Fe–Co interactions.

Fig. 6 exhibits the O 1s XPS for 7Fe3Co700. Besides the main peak at 529.7 eV corresponding to lattice oxygen species, a shoulder at higher binding energy of 531.8 eV is identified to surface hydroxyl groups (i.e. Fe–OH and Co–OH) [9]. The content of surface hydroxyl oxygen in the total oxygen for 3Fe7Co700, 1Fe1Co700, and 7Fe3Co700 is 8.6, 11.0, and 16.1% respectively, as

shown in Table 1. The catalyst with a higher Fe content tended to have a larger amount of surface hydroxyl groups. Thus, one can infer that coupling of Co(II) with Fe(III) might be an effective way to increase the formation of Co(II)–OH complexes, which is a critical step for improving the catalytic activity of Co catalyst (discussed in details in Section 3.5) [9,14].

3.4. Degradation of 2,4-DCP and cobalt leaching

The 2,4-DCP degradation profiles in the systems of 1Fe1Co catalysts, Fe₂O₃, Co₃O₄, and physical mixture of Fe₂O₃ and Co₃O₄ (mole ratio of Fe/Co = 1) are shown in Fig. 7. The bulk Fe₂O₃ could not activate PMS (Fig. 7a) since Fe(III) in Fe₂O₃ does not act as an electron donor to activate PMS. In contrast, a relatively faster 2,4-DCP degradation kinetics was achieved in Co₃O₄ system with Co(II) species (Fig. 7c). It is interesting that the 1Fe1Co catalysts are more effective than both the bulk Co₃O₄ and the physical mixture of Fe₂O₃ and Co₃O₄ (Fig. 7b). This implies the crucial role of Fe–Co interactions on the efficient PMS activation over the Fe–Co catalysts. In our previous study [9], we addressed the effect of homogeneous reaction resulting from dissolved Co(II) ions on heterogeneous PMS activation, and found that 36 µg/L of Co(II) ions could only induce around 10% of 2,4-DCP degradation within 2 h under the identical experimental conditions used in this study. In addition, it should be noted that the cobalt leaching from 1Fe1Co catalysts was fairly low between 30 and 40 µg/L (Fig. 8). This means the influence of homogeneous PMS activation due to the leached Co(II) ions on the degradation of 2,4-DCP in the 1Fe1Co

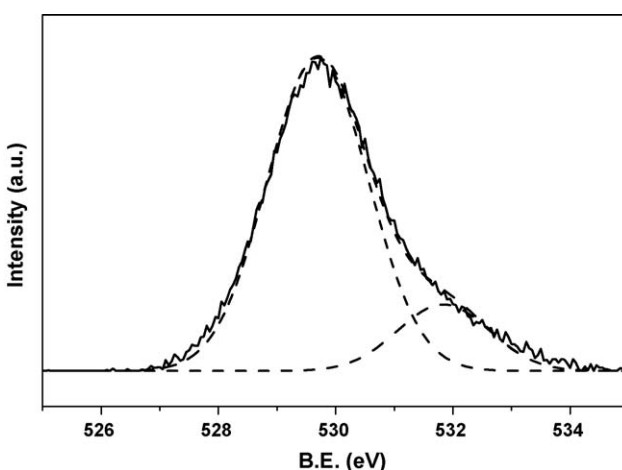


Fig. 6. XPS spectra of O 1s for 7Fe3Co700.

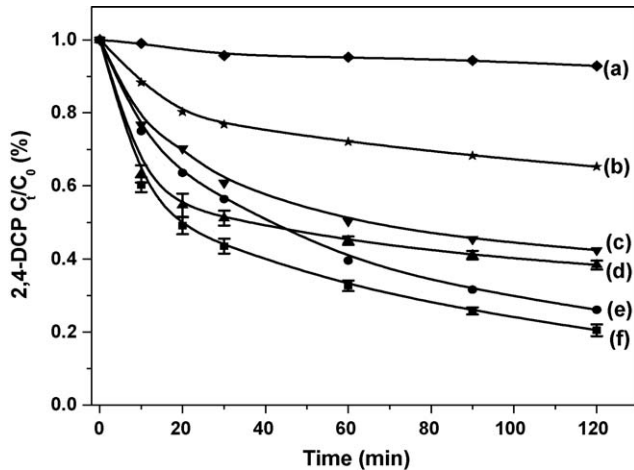


Fig. 7. 2,4-DCP transformation using (a) Fe_2O_3 , (b) $\text{Fe}_2\text{O}_3 + \text{Co}_3\text{O}_4$ (Fe:Co = 1:1), (c) Co_3O_4 , (d) 1Fe1Co700 , (e) 1Fe1Co300 , and (f) 1Fe1Co500 . The error bars indicate the standard deviations of triplicated results.

systems was not significant. It is quite worthwhile to note that the catalytic activity of 1Fe1Co700 is still high in spite of its extremely small S_{BET} as compared with 1Fe1Co300 and 1Fe1Co500 (Fig. 7d). As revealed by previous studies, Co(II) is the most efficient species for PMS activation to generate highly oxidizing SRs [11,14] while Co(III) is unable to directly activate PMS because it needs to be reduced to Co(II) with the expense of PMS consumption by forming much less reactive peroxymonosulfate radicals (SO_5^{\bullet}) [14]. Cobalt in 1Fe1Co300 and 1Fe1Co500 exists as Co_3O_4 (i.e. $\text{CoO}\text{-Co}_2\text{O}_3$) and thus Co(III) is dominant, whereas 1Fe1Co700 contains significant content of CoFe_2O_4 where Co species is of Co(II) [28]. The relatively higher concentration of Co(II) in 1Fe1Co700 compensates its much low S_{BET} , which can explain its high catalytic activity on heterogeneous PMS activation. After 2 h reaction, around 40% mineralization of 2,4-DCP could be achieved with the Fe-Co catalysts. Furthermore, a previous study in our group has clearly revealed that in the aqueous homogeneous Co^{2+} /PMS system, the major reaction intermediates during 2,4-DCP degradation by sulfate radical attack were 2,4,6-trichlorophenol, 2,3,5,6-tetrachloro-1,4-benzenediol, 1,1,3,3-tetrachloroacetone, pentachloroacetone, and carbon tetrachloride [10]. We expect that the major reaction intermediates in the present study should be similar to the above-mentioned species identified in the aqueous homo-

geneous Co^{2+} /PMS system; however, the degradation pathway of 2,4-DCP might be slightly different between the homogeneous (Co^{2+} /PMS) and heterogeneous (Fe-Co catalysts/PMS) systems. Therefore, detailed studies will be performed to identify various reaction intermediates of 2,4-DCP degradation in heterogeneous Fe-Co catalysts/PMS systems in future.

As shown in Fig. 8, all the catalysts displayed fairly low Co leaching between 20 and 50 $\mu\text{g/L}$ except FeCo/TiO_2 . Furthermore, it should be noted that 7Fe3Co700 exhibited the lowest cobalt leaching mainly due to the efficient formation of CoFe_2O_4 . Given the effectiveness of Co(II) on PMS activation, Anipsitakis et al. investigated the feasibility of using CoO for heterogeneous PMS activation [12]. However, they observed extremely high concentration of dissolved cobalt (at neutral pH). On the contrary, Co_3O_4 , where CoO is bound to Co_2O_3 , showed a better performance for the heterogeneous PMS activation due to the intimate interactions between CoO and Co_2O_3 . Nonetheless, the presence of abundant Co(III) species in Co_3O_4 is able to impair the overall efficiency for PMS activation because of the reaction between Co(III) and PMS to form much less reactive SO_5^{\bullet} . The CoFe_2O_4 in 1Fe1Co700 catalysts successfully overcame the limitations above as Co species in CoFe_2O_4 are of Co(II).

3.5. Role of Fe-Co interactions on heterogeneous PMS activation

The intimate Fe-Co interactions, due to the formation of CoFe_2O_4 in 1Fe1Co700 , are considered to be very critical for efficient heterogeneous coupling of PMS with the catalyst. The rate-limiting step for Co(II)-mediated PMS activation is the generation of Co(II)-OH complexes derived from H_2O dissociation with Co(II) ($\text{Co}^{2+} + \text{H}_2\text{O} \leftrightarrow \text{CoOH}^+ + \text{H}^+$) [11,14]. Our previous study has demonstrated that Co_3O_4 is inferior in this process since the Co(II)-OH complexes are hardly regenerated once they are consumed [9]. Previous studies showed that immobilization of Co_3O_4 on TiO_2 is effective for enhancing the formation of Co(II)-OH complexes because of the strong ability of TiO_2 to dissociate H_2O [29,30]. In the Co/TiO_2 system, H_2O is readily dissociated to generate hydroxyl groups on the TiO_2 surfaces, and Co species might interact with the nearby surface hydroxyl groups on the TiO_2 support, rather than directly with H_2O , to form Co(II)-OH complexes [9]. This pathway guarantees the continuous generation of Co(II)-OH complexes along with their consumption during the PMS activation. In a similar way, the promotion effect of Fe(III) on the regeneration of Co(II)-OH complexes is expected in 1Fe1Co700 , as demonstrated in the following reactions:

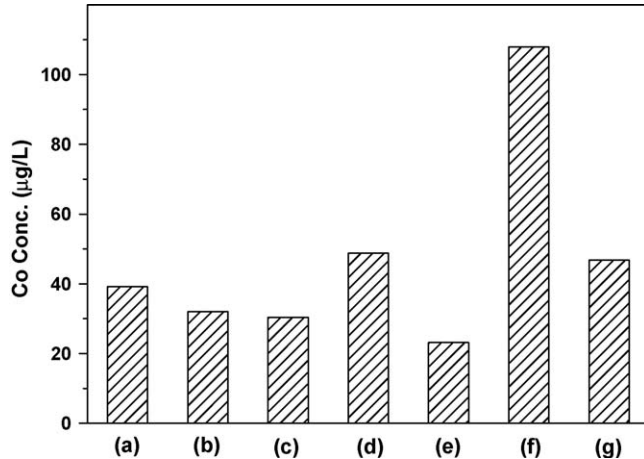
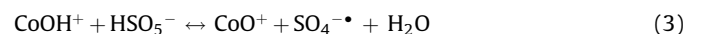
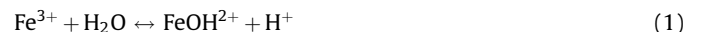


Fig. 8. Concentration of leached cobalt after 2 h of reaction in the systems of (a) 1Fe1Co300 , (b) 1Fe1Co500 , (c) 1Fe1Co700 , (d) 3Fe7Co700 , (e) 7Fe3Co700 , (f) FeCo/TiO_2 , and (g) 0.1Co/TiO_2 .

Lin et al. have reported the extraordinary capability of Fe(III) to form Fe(III)-OH complexes via H_2O dissociation [31], which is consistent with our XPS results that show the Fe-Co catalysts containing more Fe possess higher content of surface hydroxyl groups. We therefore believe that over CoFe_2O_4 , H_2O should be preferentially dissociated on Fe(III) (Reaction (1)) compared with Co(II). Thus, it is very likely that Co(II) can readily interact with the nearby surface hydroxyl groups bound to Fe(III) to form Co(II)-OH (Reaction (2)) due to the intimate Fe-Co interactions in CoFe_2O_4 . Such a route can effectively replenish the Co(II)-OH complexes over 1Fe1Co700 during their consumption over PMS activation (Reaction (3)). Consequently, it is evident that Fe(III) in CoFe_2O_4 acts as a reservoir of "OH" species, which can be effectively utilized

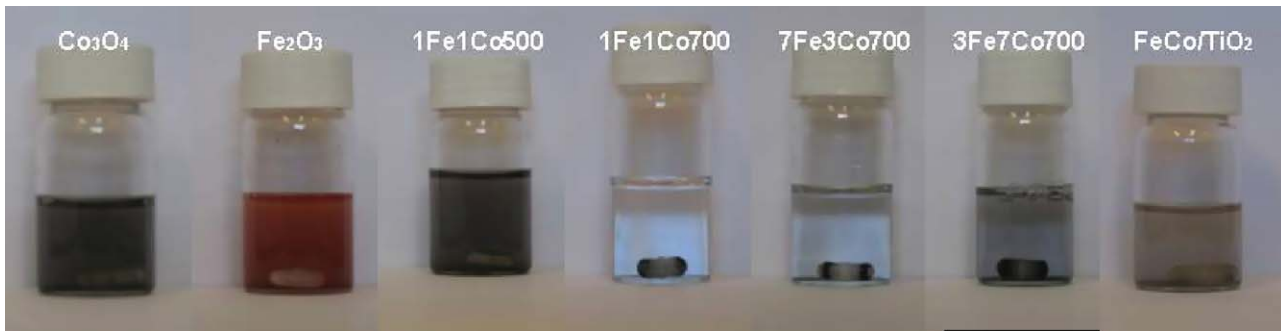


Fig. 9. Illustration of the magnetic separation of the Fe-Co nanocomposite catalysts from the aqueous environments.

by Co(II) to facilitate the activation of PMS. This hypothesis is strongly supported by two facts: (i) the inferior catalytic performance of the physical mixture of Fe_2O_3 and Co_3O_4 (Fig. 7b), in which no intimate Fe–Co interactions were generated, and (ii) Fe–Co catalysts (Fig. 7f and d) exhibited better activities than Co_3O_4 (Fig. 7c) with higher cobalt content.

3.6. Ferromagnetic properties and environmentally friendly aspects

As exhibited in Fig. 9, 1Fe1Co700 could be readily separated from the solution using a magnetic stirrer bar due to the exceptional ferromagnetic nature of CoFe_2O_4 , unlike other catalysts such as Co_3O_4 , Fe_2O_3 , and 1Fe1Co500. 1Fe1Co700 catalyst showed effective heterogeneous PMS activation and possesses environmentally benign characteristics such as reduced cobalt leaching and easy recovery features. Traditionally, immobilization of nanosized catalytic particles onto substrates has been considered as one of the most practical ways to prevent them from being released into aqueous environments [32,33]. However, this approach suffers from progressive decrease in catalytic activity largely due to the formation of passivation layers on the catalysts (i.e. called fouling and deactivation) and consequently the whole catalytic coating has to be replaced. Supporting the Fe–Co catalysts on magnetic materials can give us a satisfactory solution to this issue and seems to be practical for wastewater treatments because it is relatively easier to separate the Fe–Co catalysts based magnetic materials as compared with the conventional coating approach.

FeCo700 catalysts with different Fe/Co ratios exhibited very similar activities in spite of much lower cobalt content of

7Fe3Co700 (Fig. 10). This might be interpreted from two aspects: (i) all the cobalt species in 7Fe3Co700 are of Co(II) in form of CoFe_2O_4 and (ii) 7Fe3Co700 contained the highest amount of iron which facilitates the formation of surface hydroxyl groups. In addition, the separation of 3Fe7Co700 from the solution was not as good as that of 7Fe3Co700 and 1Fe1Co700 (Fig. 9) due to the co-existence of abundant Co_3O_4 in 3Fe7Co700. Considering its magnetic separation behavior, cobalt leaching properties, and relatively high activity, 7Fe3Co700 is the most environmentally friendly of the catalytic materials synthesized in this study and recommended for further optimization (e.g. development of novel approaches by which high-surface-area CoFe_2O_4 can be synthesized at much lower temperatures) and studies in relevant environmental applications.

3.7. Immobilization of Fe–Co nanocomposites on TiO_2 support

The Fe–Co nanoparticles were further immobilized onto TiO_2 surface since immobilization of Co_3O_4 onto TiO_2 was reported to be effective for reducing cobalt leaching and enhancing its performance on heterogeneous PMS activation [8]. As shown in Fig. 11, FeCo/TiO₂500 and 0.1Co/TiO₂ exhibited similar catalytic activities, which were apparently higher than that of 1Fe1Co500. However, the cobalt leaching from FeCo/TiO₂500 was much larger than that of either 0.1Co/TiO₂ or 1Fe1Co500 (Fig. 8). This suggests that the presence of TiO_2 could hinder the formation of intimate Fe–Co interaction. Moreover, as shown in Fig. 9, FeCo/TiO₂700 could not be effectively separated from the solution due to the presence of abundant TiO_2 .

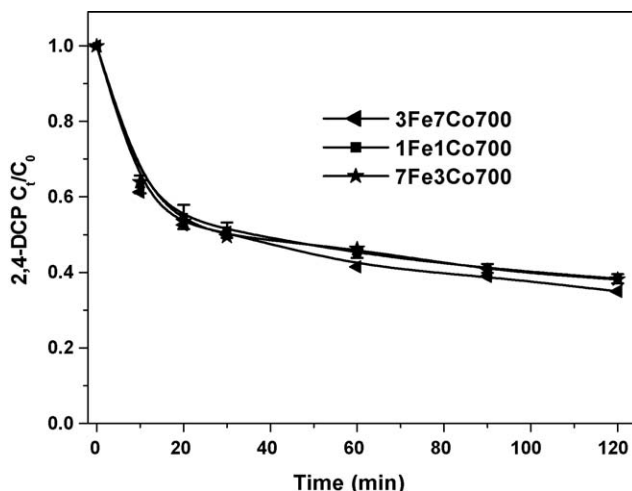


Fig. 10. 2,4-DCP transformation with Fe–Co catalysts calcined at 700 °C.

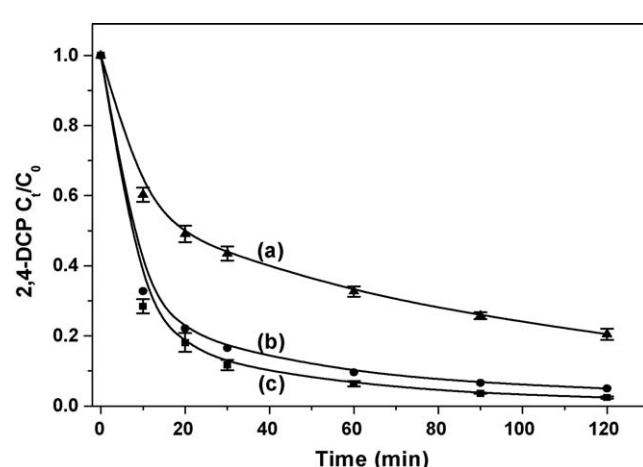


Fig. 11. 2,4-DCP transformation using (a) 1Fe1Co500, (b) FeCo/TiO₂500, and (c) 0.1Co/TiO₂.

4. Conclusions

In the present study, efficient and environmental benign (i.e. minimum cobalt leaching and recoverable features) Fe–Co mixed oxide nanocatalysts have been developed for heterogeneous activation of peroxyomonosulfate (PMS) to generate SRs targeting the decomposition of 2,4-DCP. It was clearly revealed that both Fe/Co molar ratio and calcination temperature were of crucial importance for the catalyst performance. In 7Fe3Co700 (Fe:Co = 7:3, calcined at 700 °C) catalyst, ferromagnetic CoFe₂O₄ composites effectively formed by thermal oxidation of a mixed phase of Fe and Co. It was found that this catalyst is the most promising for the efficient and environmentally friendly activation of PMS because of its exceptional physicochemical properties including (i) the cobalt species in CoFe₂O₄ are of Co(II), unlike Co₃O₄ that shows some limitation of Co(III) on PMS activation, (ii) CoFe₂O₄ possesses suppressed Co leaching properties due to strong Fe–Co interaction (Fe–Co linkages), and (iii) Fe–Co catalysts in form of CoFe₂O₄ are easy to recover due to the unique ferromagnetic nature of CoFe₂O₄. Moreover, XPS results demonstrated that the conjunction of Co with Fe is beneficial for enhancing the content of hydroxyl groups on the catalyst surface, which is believed to facilitate the formation of Co(II)–OH complexes that are vital for heterogeneous PMS activation. In addition, immobilization of Fe–Co catalyst on TiO₂ support was attempted for further suppressing the cobalt leaching. Contrary to our expectation, the immobilized catalyst FeCo/TiO₂ exhibited very high cobalt leaching, which suggests that the presence of TiO₂ could hinder the formation of intimate Fe–Co interaction.

Acknowledgments

The authors are grateful to the National Science Foundation through a CAREER Award (BES-0448117), to DuPont through a Young Professor Award to D.D. Dionysiou, and the National Risk Management Research Laboratory of EPA, Cincinnati, Ohio for financial support for this study (EP-C-05-056). This paper has not been subjected to internal policy review of the U.S. Environmental Protection Agency (EPA). Therefore, the research results do not

necessarily reflect the views of the agency or its policy. Mention of trade names and commercial products does not constitute endorsement or recommendation for use.

References

- [1] S. Malato, J. Blanco, C. Richter, B. Braun, M.I. Maldonado, *Appl. Catal. B: Environ.* 17 (1998) 347.
- [2] M. Pera-Titus, V. García-Molina, M.A. Baños, J. Giménez, S. Esplugas, *Appl. Catal. B: Environ.* 47 (2004) 219.
- [3] M.R. Hoffmann, S.T. Martin, W. Choi, D.W. Bahnemann, *Chem. Rev.* 95 (1995) 69.
- [4] Q. Yang, Z. Xu, C. Xie, Z. Gao, Y. Du, *J. Phys. Chem. B* 109 (2005) 5554.
- [5] C. Xie, Q. Yang, Z. Xu, X. Liu, Y. Du, *J. Phys. Chem. B* 110 (2006) 8587.
- [6] A. Safarzadeh-Amiri, J.R. Bolton, S.R. Cater, *J. Adv. Oxid. Technol.* 1 (1996) 18.
- [7] P. Neta, R.E. Huie, A.B. Ross, *J. Phys. Chem. Ref. Data* 17 (1988) 1027.
- [8] Q. Yang, H. Choi, Y. Chen, D.D. Dionysiou, *Appl. Catal. B: Environ.* 77 (2008) 300.
- [9] Q. Yang, H. Choi, D.D. Dionysiou, *Appl. Catal. B: Environ.* 74 (2007) 170.
- [10] G.P. Anipsitakis, D.D. Dionysiou, M.A. Gonzalez, *Environ. Sci. Technol.* 40 (2006) 1000.
- [11] G.P. Anipsitakis, D.D. Dionysiou, *Environ. Sci. Technol.* 37 (2003) 4790.
- [12] G.P. Anipsitakis, E. Stathatos, D.D. Dionysiou, *J. Phys. Chem. B* 109 (2005) 13052.
- [13] G.P. Anipsitakis, D.D. Dionysiou, *Appl. Catal. B: Environ.* 54 (2004) 155.
- [14] G.P. Anipsitakis, D.D. Dionysiou, *Environ. Sci. Technol.* 38 (2004) 3705.
- [15] J. Fernandez, P. Maruthamuthu, A. Renken, J. Kiwi, *Appl. Catal. B: Environ.* 49 (2004) 207.
- [16] M.R. Wiesner, G.V. Lowry, P. Alvarez, D.D. Dionysiou, P. Biswas, *Environ. Sci. Technol.* 40 (2006) 4336.
- [17] A. Nel, T. Xia, Lutz Mädler, N. Li, *Science* 311 (2006) 622.
- [18] R.J. Griffitt, R. Weil, K.A. Hyndman, N.D. Denslow, K. Powers, D. Taylor, D.S. Barber, *Environ. Sci. Technol.* 41 (2007) 8178.
- [19] J. Zhou, H. He, Y. Lin, C. Nan, Mater. Lett. 60 (2006) 1542.
- [20] Ø. Borg, S. Eri, E.A. Blekkan, S. Storsæter, H. Wigum, E. Rytter, A. Holmen, *J. Catal.* 248 (2007) 89.
- [21] S. Kim, S. Lee, S. An, C. Kim, *J. Magn. Magn. Mater.* 215–216 (2000) 210.
- [22] V. Barrón, J. Torrent, E. De Grave, *Am. Miner.* 88 (2003) 1679.
- [23] E. Rombia, I. Ferino, R. Monaci, C. Picciu, V. Solinas, R. Buzzoni, *Appl. Catal. A: Gen.* 266 (2004) 73.
- [24] M. Kraum, M. Baerns, *Appl. Catal. A: Gen.* 186 (1999) 189.
- [25] A. Lapidus, A. Krylova, V. Kazanskii, V. Borovkov, A. Zaitsev, J. Rathousky, A. Zukal, M. Jančáková, *Appl. Catal.* 73 (1991) 65.
- [26] G.A. El-Shobaky, M.A. Shouman, M.N. Alaya, *Adsorp. Sci. Technol.* 18 (2000) 243.
- [27] R. Xu, H. Zeng, *Langmuir* 20 (2004) 9780.
- [28] X. Yang, X. Wang, Z. Zhang, *J. Crystal Growth* 277 (2005) 467.
- [29] A.L. Linsebigler, G. Lu, J.T. Yates Jr., *Chem. Rev.* 95 (1995) 735.
- [30] M.A. Henderson, *Surf. Sci. Rep.* 46 (2002) 1.
- [31] S. Lin, M.D. Gurrol, *Environ. Sci. Technol.* 32 (1998) 1417.
- [32] Y. Chen, D.D. Dionysiou, *Appl. Catal. B: Environ.* 62 (2006) 25.
- [33] Y. Chen, D.D. Dionysiou, *Appl. Catal. B: Environ.* 69 (2006) 24.